Research Article Vol. 3, No. 7 / 15 Jul 2024 / Optics Continuum 1116
OPTICS CONTINUUM

# Trident edge coupler on thin-film lithium niobate for optimized coupling of octave-separated wavelengths for nonlinear applications

JOHN O. GERGUIS,* GREGORY CHANG, AND MINGHAO QI

*School of Electrical and Computer Engineering, Purdue University, West Lafayette, Indiana, 47907, USA*
*jgerguis@purdue.edu*

**Abstract:** We introduce a trident edge coupler design optimized for the simultaneous coupling of two widely separated wavelengths (2 μm and 1 μm) between a lensed fiber and a 600-nm-thick X-cut lithium-niobate-on-insulator (LNOI) waveguide. These wavelengths are commonly encountered in nonlinear wave mixing applications, representing either the fundamental and second harmonics in second harmonic generation (SHG) processes or the leading and trailing edges of an octave-spanning spectrum generated through broadband nonlinear processes such as frequency comb or supercontinuum generation. Achieving efficient coupling between fibers and strongly confined waveguides in integrated platforms, such as LNOI, can be challenging due to the significant difference in spot sizes between the two wavelengths. Our trident edge coupler offers coupling losses below 1.4 dB for the 2 μm and 1 μm spots simultaneously, showcasing an average transmission enhancement of around 10% compared to the baseline of a single linear taper. Furthermore, it enables a reduction of transmission at 1.5 μm, a typical pump wavelength, with an attenuation of transmission over 10 dB compared to those at the 2 μm and 1 μm wavelengths.



## 1. Introduction

Photonic integrated circuits (PICs) have benefited greatly from the advancement in their volume manufacturing and are in a position to start replacing bulk optics in many applications including frequency combs [1], LiDARs [2–4], sensing and biomedical applications [5,6], photonic computing [7,8], and RF photonics [9–11] for their advantages of small footprints and stability of performance enabled by integration. Different silicon-based platforms, including $SiO_2$ and SiN have been intensively used because of their compatibility with CMOS technology. Lithium Niobate ($LiNbO_3$, LN) has been studied since the 1960s and has been attractive owing to its electro-, nonlinear-, and acousto-optic properties, in addition to its high refractive index and wide range of wavelength transparency [12]. Lithium Niobate garnered more attention since the early 2000s, when thin-film LN wafers prepared through ion splicing and wafer bonding have been made commercially available [13,14].

Coupling of light to PIC chips from optical fibers is required in most applications. The advancement of the integrated nonlinear devices calls for improved optical interconnects suitable to couple lights from nonlinear processes, such as second harmonic generation (SHG), sum frequency generation (SFG), and difference frequency generation (DFG) processes, in which the wavelengths are widely separated, *e.g.* by an octave. While coupling of extremely broadband light, *e.g.*, octave-spanning frequency combs or supercontinuum, from waveguides to lensed fibers have been reported [15], systematic modeling and optimization of coupling at octave-separated wavelengths with different spot sizes, to the best of our knowledge, has not been reported. Limited information on coupling performance in the literature exists for such applications. The prevailing belief is that a single taper represents the simplest coupler design capable of facilitating reasonable coupling for such applications. However, as we will point out in Fig. 4, the optimal coupling conditions for the 1 μm and 2 μm wavelengths with different spot sizes are conflicting

#518712 https://doi.org/10.1364/OPTCON.518712
Journal © 2024 Received 11 Jan 2024; revised 11 Apr 2024; accepted 16 Apr 2024; published 15 Jul 2024

OPTICS CONTINUUM

with each other and a trade-off has to be made. This also led us to select the compromised single inverse taper as a baseline in this paper, enabling a comparison of the performance of our design.

There are generally two categories of fiber-to-chip coupling. Grating couplers [16] are widely used due to their manufacturing advantages and the ability to couple an array of fibers to multiple waveguides simultaneously. However, these structures are wavelength-selective, posing a challenge in their design when employed in nonlinear applications that necessitate the simultaneous coupling of multiple wavelengths. Edge couplers [17] are the other approach which have the advantages of wider bandwidth and being less polarization dependent compared to grating couplers, which makes them more suitable for nonlinear applications.

Different structures of edge couplers have been intensively studied recently. The most widely used form of edge couplers is based on inverse tapering [18], where the narrower tip of the taper faces the fiber, and the width of the taper increases gradually towards the chip, to be able to accommodate the output mode from the fiber and adiabatically convert it to the mode of the integrated waveguide. Multiple-taper couplers were developed, that allowed higher mode overlap efficiency with the fiber, and more tolerance to the misalignment between the fiber and the chip [18]. The trident edge coupler is one of the most used forms for multiple-taper edge couplers, which consists of two auxiliary tapers on both sides of the middle one [19]. The structure offers the flexibility to design the spacings between the separate tapers, as well as their tip widths, *etc*. As a result, it could potentially match two or more spot sizes at different wavelengths from the same fiber.

The power coupled to the trident edge coupler is distributed among the three tapers and needs to be combined into one output waveguide before entering the chip. Different power combination techniques have been explored previously. The most widely used technique is through the evanescent coupling of light from the auxiliary tapers towards the middle one [20]. A broadband edge coupler on TFLN based on the evanescent coupling of light from the auxiliary tapers was presented and experimentally demonstrated in [21] as well. Power combination from auxiliary tapers was also demonstrated using simple Y-junctions [22,23]. Multi-mode interference (MMI) was introduced to combine the power into an output waveguide [18,24,25].

Previously reported edge coupler designs typically focused on optimizing coupling for a specific wavelength. To achieve optimal coupling for different wavelengths, it's essential that the expanded mode profile of the taper tip closely matches the mode of the lensed fiber at its focal spot for each specific wavelength. In response to these considerations, we present an optimized trident edge coupler design that efficiently couples light from a lensed fiber with varying spot sizes at different wavelength bands. The simulation was performed using the commercial software Ansys Lumerical FDTD Solutions. Our proposed design is capable of coupling light from a lensed fiber at two different wavelengths, specifically 2 μm and 1 μm, which are the target wavelengths for coupling. Additionally, we address the intermediate wavelength of 1.5 μm, which in many cases represents the pump wavelength, all propagating through an X-cut Lithium-Niobate-On-Insulator (LNOI) waveguide with a film thickness of 600 nm.

This design is particularly relevant in broadband, *e.g.* octave-spanning, nonlinear applications such as frequency combs, supercontinuum generation [15], and spontaneous down conversion, where the intensity in the output spectrum peaks at the pump wavelength and decreases away from the pump towards the edges of the spectrum. In many scenarios, it might be advantageous to reduce the coupling around the corresponding pump wavelength, *e.g.* at 1.5 μm to achieve a partial spectral equalization. In scenarios involving the on-chip generation of nonlinear processes, our coupler would assume a role at the output, where it spectrum-shapes and couples light to the fiber. It could prove advantageous to incorporate frequency comb generation [27] or supercontinuum generation [15] directly onto the LN chip. This integration could facilitate further processing, such as for optical communication systems, enabling the full system to be seamlessly integrated onto a single chip. Additionally, the utilization of second harmonic generation through

OPTICS CONTINUUM

periodically poled LN waveguides for f-2f referencing of frequency combs presents another compelling application, further highlighting the potential interest in having frequency comb generation on the same LN chip. However, the coupler's utility extends to diverse applications, including serving as broadband input coupling to, for example, on-chip spectrometers, where the ability to shape the spectrum during the coupling process onto the chip would potentially ease the requirements associated with accommodating high power dynamic ranges, *i.e.* attenuate the pump wavelength and enhance the coupling at the leading and trailing wavelengths.

The rest of the paper is organized as follows. First, in section 2, a theoretical study is presented on the ratios of the output spot sizes from the lensed fiber at the wavelengths of interest to get an insight into the expected spot size range. In section 3, the structure of the proposed trident edge coupler is presented, and the design procedure is explained. In section 4, simulation results for the structure are presented, including its performance across selected wavelength ranges, and its tolerance to the input fiber misalignment and fabrication variations around the wavelengths of interest. Finally, the work is concluded in section 5.

## 2. Output spot sizes from lensed fibers versus wavelength

The modes supported by integrated waveguides have small spot sizes compared to the mode field diameter (MFD) of the cleaved single-mode fibers (SMFs). Typically, lensed or tapered fibers are used to couple light from the fibers to the chip [26]. These fibers are manufactured either by laser shaping the end facet of the fiber or by polishing it to form a lens of a specific radius and taper angle. An output spot of a diameter as small as a few micrometers can be achieved by the lensed fibers, which makes them suitable for coupling with the PICs [26].

The available off-the-shelf fibers might not be able to operate across the whole wavelength bands of interest, *i.e.* 1–2 μm, while maintaining low losses. Typical Silica fibers, for instance, commonly exhibit relatively high attenuation at 2 μm, and detailed information about the spot size at 2 μm from the available silica fibers may not be readily accessible. In cases where fiber loss is a critical consideration, specialty fibers tailored to the specific application and required wavelengths might be necessary. Alternatively, the use of silica fibers could be considered, albeit at the expense of higher attenuation in the long-wavelength range. The design of the edge coupler is dependent on the spot sizes, so they need to be known before designing the structure. In practice, the output spot sizes from the lensed fiber can typically be obtained from the manufacturer. Alternatively, if these spot sizes are not readily available, experimental characterization becomes necessary. This involves employing a beam profiler to measure the cross-sectional dimensions of the spots at the desired wavelengths. Such characterizations ensure accurate and precise design parameters for the edge coupler.

In this study, we provide a theoretical estimation of the range of spot size ratios at wavelengths of 2 μm and 1 μm, forming the foundation for our design. We selected this wavelength pair as they represent the leading and trailing edges of an on-chip frequency comb, primarily pumped near the 1.5 μm wavelength [1,27]. To simplify the analysis, we employ a model of the lensed fiber illustrated in Fig. 1. We assume that the output from the fiber travels a certain distance, denoted as L, before encountering the lens, which has a radius of curvature represented by R. The materials constituting the propagation medium preceding the lens and the lens itself are assumed to have the same refractive index as the fiber's cladding, specifically, $n_{clad} = 1.437$. This theoretical framework guides our subsequent design and analysis.

The output spot of the fundamental mode from a fiber should possess a mode field diameter, which can be approximated using Marcuse's equation [28]:

$$MFD = 2a\left(0.65 + \frac{1.619}{V^{3/2}} + \frac{2.879}{V^6}\right) \tag{1}$$

OPTICS CONTINUUM

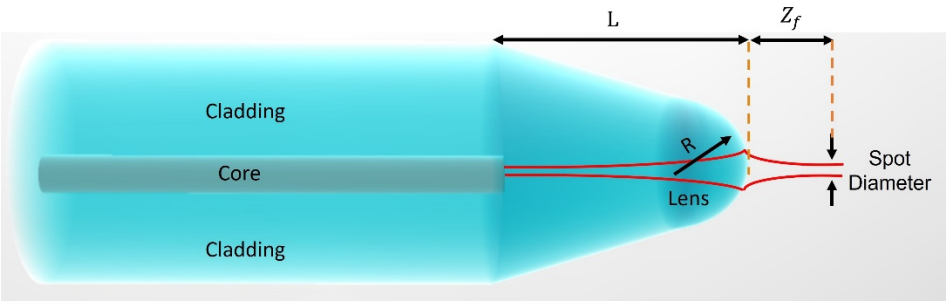


**Fig. 1.** Schematic for the lensed fiber used in the model.

where $a$ is the core radius of the fiber, and V is the normalized frequency given by:

$$V = \frac{2\pi}{\lambda} a\, NA, \tag{2}$$

where λ is the wavelength of light and NA is the numerical aperture of the fiber ($NA = \sqrt{n_{core}^2 - n_{clad}^2}$, where $n_{core}$ *and* $n_{clad}$ are the refractive indices of the core and the cladding, respectively). The output from the fiber is assumed to have a Gaussian beam profile with a beam waist equal to MFD/2. To simplify the analysis of light propagation through the lensed fiber and gain insight into the range of spot size ratios at 2 μm and 1 μm wavelengths, we employ ABCD matrix analysis. In this analysis, the beam exits the fiber, propagates a distance L, encounters the lens, and continues to propagate for a distance $Z_f$ beyond the lens until it reaches the focus, which is the position of the minimum waist. The collective ABCD matrix for this system can be described by the multiplication between the ABCD matrices for the propagation in air for a distance $Z_f$, the lens, and the propagation in the cladding for a distance L as follows:

$$\begin{aligned}\begin{bmatrix} A & B \\ C & D \end{bmatrix}_{Total} &= \begin{bmatrix} 1 & Z_f \\ 0 & 1 \end{bmatrix} \times \begin{bmatrix} 1 & 0 \\ \frac{n_{clad}-1}{R} & n_{clad} \end{bmatrix} \times \begin{bmatrix} 1 & L \\ 0 & 1 \end{bmatrix} \\ &= \begin{bmatrix} 1 + (n_{clad}-1)\frac{Z_f}{R} & L + (n_{clad}-1)\frac{Z_f}{R}L + n_{clad}Z_f \\ \frac{n_{clad}-1}{R} & \frac{n_{clad}-1}{R}L + n_{clad} \end{bmatrix},\end{aligned} \tag{3}$$

After mathematical manipulations following [29], $Z_f$ can be calculated as:

$$Z_f = \frac{\frac{(1-n_{clad})}{R}\left(\frac{\pi^2 MFD^4}{16\lambda^2}\right) + \frac{(1-n_{clad})}{R}L^2 - n_{clad}L}{\left[\frac{(n_{clad}-1)}{R}L + n_{clad}\right]^2 + \frac{(n_{clad}-1)^2}{R^2}\left(\frac{\pi^2 MFD^4}{16\lambda^2}\right)} \tag{4}$$

After the propagation of the Gaussian beam (output from the fiber) through the ABCD matrix, the spot diameter at the focus of the lensed fiber is given by:

$$Spot\ Diameter\ (SD) = \sqrt{\frac{MFD^2(AD-BC)}{(D^2 + AC\pi^2 MFD^4/16\lambda^2)}}, \tag{5}$$

where MFD, A, B, C and D were defined in the previous relations. The Spot Diameter (SD) provided by this equation is applicable under the paraxial approximation, which assumes that the

OPTICS CONTINUUM

beam is closely aligned with the lens axis. In practical scenarios, lensed fibers often have very small radii within the range of a few micrometers, where the paraxial approximation is not valid. To gain a rough estimate of the range of spot diameter ratios at wavelengths of 2 μm and 1 μm, we perform calculations with relatively larger values of R. The purpose is to gain insights into the spot diameter ratios. For the calculations, we assume an absolute spot diameter at $\lambda = 1$ μm of 2 μm, a value that falls within the range of output spot diameters typically associated with commercial lensed fibers. Consequently, the spot diameter at $\lambda = 2$ μm is determined based on this ratio.

The ratios of the spots of the fundamental modes at the wavelengths 2 μm and 1 μm are plotted vs the parameters of the fiber and the lens. Figure 2 shows the variation of the ratio vs the fiber NA at a core radius of 4.1 μm (the typical core radius of the commercial Corning SMF-28 fiber). Figure 2(a) shows the variation at different distances L for R = 62.5 μm, while Fig. 2(b) shows the variation at different lens radii of curvature R for L = 62.5 μm, where 62.5 μm is the typical cladding radius for the commercial single-mode fibers. Figure 3 shows the variation of the ratio vs the core radius of the fiber at an NA of 0.14 (the typical NA of the commercial Corning SMF-28 fiber). Figure 3(a) shows the variation at different distances L for R = 62.5 μm, while Fig. 3(b) shows the variation at different lens radii of curvature R for L = 62.5 μm.

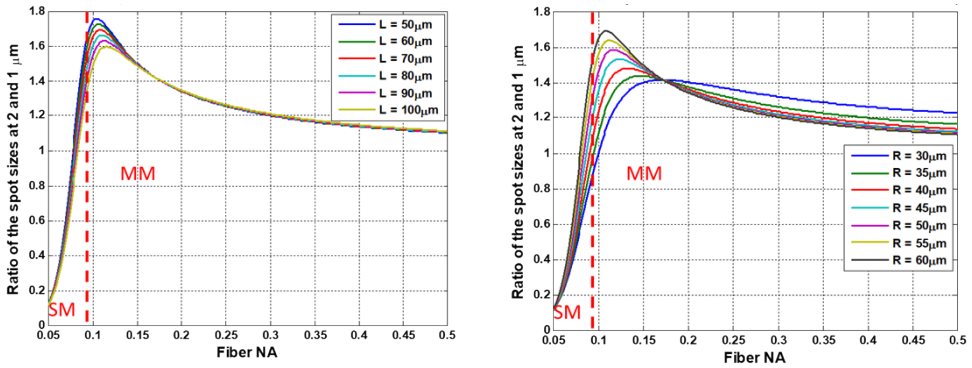


(a) (b)

**Fig. 2.** Ratio of the output spot sizes at 2 and 1 μm vs the NA of the fiber for a core radius of 4.1 μm. (a) For R = 62.5 μm at different distances L. (b) For L = 62.5 μm at different lens radii of curvature R.

In those graphs, the vertical red lines show the critical values of NA or core radius above which the fiber becomes multimode for the shorter wavelength of 1 μm. In other words, the areas to the left of these lines correspond to single-mode regions, while those on the right signify multi-mode regions. The analysis reveals that the spot size ratio can exhibit a broad range of variations influenced by fiber and lens parameters.

In particular, around the borders of the single-mode regions, such as when considering a fiber core radius of 2.5 μm, which is relevant for future fibers intended for simultaneous single-mode operation at 1 μm and 2 μm, the spot size ratio can rise to be around 2. Consequently, for the design of the edge coupler discussed in the subsequent sections, we assume a spot size ratio of 2. For the design, we also assume a spot diameter at a wavelength of 1 μm to be 2 μm, which closely aligns with the characteristics of commercial lensed fibers. Consequently, the spot diameter at a wavelength of 2 μm is presumed to be double, namely 4 μm.

OPTICS CONTINUUM

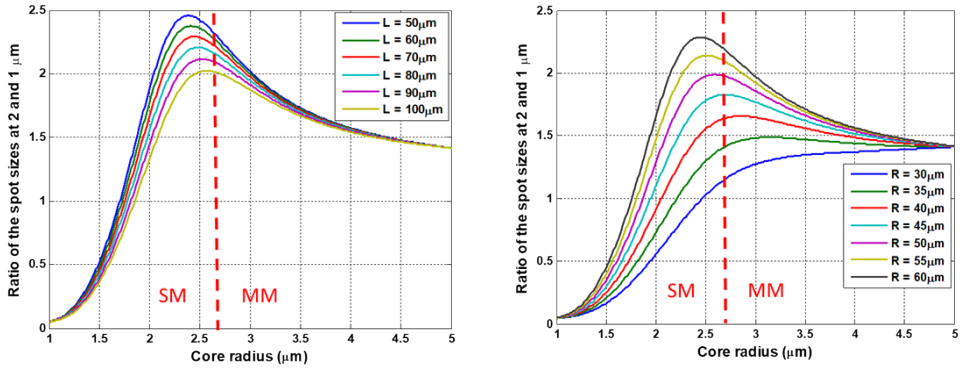


(a) (b)

**Fig. 3.** Ratio of the output spot sizes at 2 and 1 μm vs the core radius of the fiber for an NA of 0.14. (a) For R = 62.5 μm at different distances L. (b) For L = 62.5 μm at different lens radii of curvature R.

## 3. Structure

The output spot size from the fiber varies with wavelength. As per our discussion above, we assume that, to the first-order approximation, the output spots from the lensed fibers exhibit Gaussian profiles, with a linear relationship between wavelength and its minimum waist (or focal spot) size. In this study, we assign spot diameter sizes of 2 μm at a wavelength of 1 μm, 3 μm at 1.5 μm wavelength, and 4 μm at 2 μm wavelength.

Coupling two spots of different sizes using a single taper is feasible but not optimal. The challenge is elaborated in Fig. 4, where the coupling to the output waveguide of 0.6-μm width is demonstrated using a single inverse taper, representing the baseline in this investigation, for the two spots with varying lengths and tip widths. For the smaller 1 μm spot, an optimal configuration involves a narrower tip width and a longer taper, whereas the larger 2 μm spot benefits from the opposite approach. Achieving balanced coupling for both spots requires a compromise, favoring intermediate spot sizes. A single linear inverse taper of 30-μm length and 130-nm tip width is used as a baseline in this study which represents a balanced design that achieves comparable coupling at the two spots of interest.

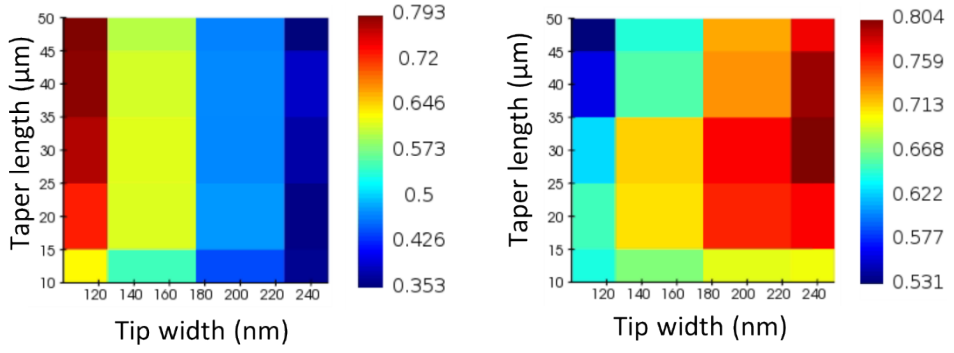


(a) (b)

**Fig. 4.** Forward transmission to the fundamental TE mode of the output waveguide of 0.6-μm width using a linear taper for various taper lengths and tip widths. (a) For the 2-μm spot at λ = 1 μm. (b) For the 4-μm spot at λ = 2 μm.

OPTICS CONTINUUM

To increase the coupling for both wavelengths, a trident coupler offers increased flexibility. In this configuration, the middle taper can be optimized for the smaller spot, while the auxiliary tapers can be tailored for the larger spot. The focal distances of the spots at the two wavelengths of 1 µm and 2 µm might be different. For simplicity and as a start, we assume that the focal distances are the same, and in Fig. 9 we show the effect of focal distance difference by varying independently the locations of the waists of the two focused Gaussian beams. In short, the penalty is small if the difference in the focal distance is small. Furthermore, if we know the difference in the focal lengths, we will be able to take that into consideration and re-optimize our design by changing the distance between the auxiliary tapers and/or introducing a recess of the middle or the auxiliary tapers.

The proposed design for the edge coupler is illustrated in Fig. 5. The representative design utilizes an X-cut Lithium-Niobate-On-Insulator (LNOI) platform with a device-layer thickness of 600 nm and $SiO_2$ cladding. The entire device is fully etched, resulting in a structure height of 600 nm. The fully etched design offers strong mode confinement, which benefits nonlinear process, and expansion of mode when inverse-tapered for highly efficient fiber coupling. Note that our design is not limited to a single device thickness of 600 nm; will demonstrate later its adaptability to other thicknesses, such as 400 nm. The design process was simulated using the commercial software Ansys Lumerical FDTD Solutions. The primary objective of the optimization process was to enhance the coupling efficiency for the two specific spots, 1 µm and 2 µm, to the fundamental TE mode of the output waveguide. Simultaneously, the design aimed to effectively attenuate the coupling of the 1.5 µm wavelength, typically representing the pump signal in broadband nonlinear mixing processes such as a frequency comb or a supercontinuum.

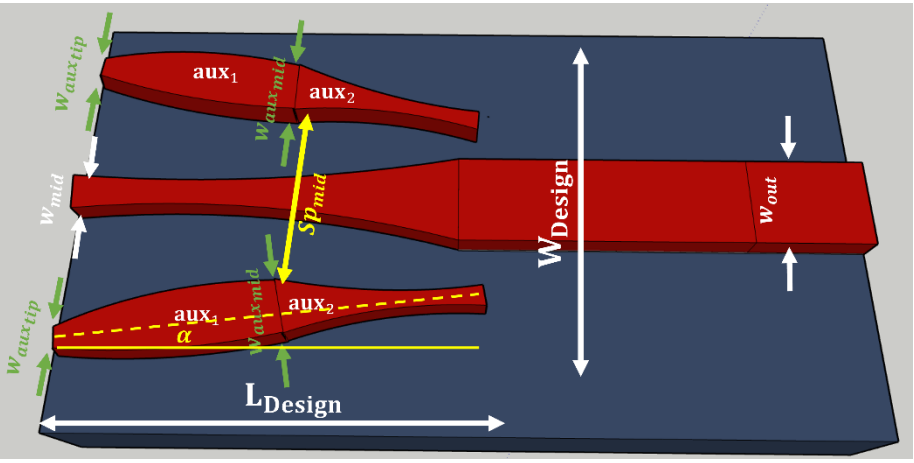


**Fig. 5.** Schematic for the proposed trident edge coupler design. $w_{mid}$ is the tip width of the middle taper, $w_{auxtip}$ and $w_{auxmid}$ are the tip and the middle widths of the auxiliary tapers, respectively, $\alpha$ is the angle of the auxiliary tapers with respect to the optical axis, $SP_{mid}$ is the spacing between the midpoints of the auxiliary tapers, $W_{Design}$ and $L_{Design}$ are the total width and length of the whole design, respectively, and $w_{out}$ is the width of the output waveguide.

Figure 5 depicts our trident input coupler. The two auxiliary tapers are placed symmetrically on both sides of the middle taper. We first optimized the coupling for the smaller spot by adjusting the tip width, length, and profile shape of the middle taper without including the auxiliary tapers. We then optimized for the coupling of the larger spot by introducing the auxiliary tapers and modifying their tip width, length, profile shape, parallelism and spacing to the middle taper. The remaining optimization process involved iterative adjustments considering the highly

OPTICS CONTINUUM

correlated interactions between these parameters. The goal was to ensure consistently high and comparable coupling efficiencies for both wavelengths/spots. The first trade-off to make was the spacing between the auxiliary tapers and the middle one, denoted by $sp_{mid}$, at midpoints of the auxiliary tapers in Fig. 5. The smaller spot favors a wider spacing so that the optical mode does not "feel" the existence of the auxiliary tapers, whereas the larger spot benefits from a narrower spacing. Consequently, a compromised spacing, $sp_{mid} = 2.4\,\mu m$ was selected to ensure comparable performance for both spots. We also found that slightly rotating the auxiliary tapers so that they converge slightly toward the middle taper would increase the coupling efficiency, and the optical angle was found to be $\alpha = 0.6°$.

Incorporating curved tapers was observed to provide a slight enhancement in performance while maintaining a compact design. The middle and auxiliary tapers were designed with curved profiles, where the widths of these profiles along the propagation distance x adhere to the following relation:

$$w(x) = \kappa(L - x)^m + w_2 \tag{6}$$
$$\kappa = \frac{w_1 - w_2}{L^m}$$

where $w_1$ and $w_2$ represent the initial and end widths on the left and right sides of the taper, L denotes its length, and m is a parameter defining the taper profile. The design's parameters and dimensions are summarized in Table 1. The middle taper features a length of $L_{mid}$ and $m_{mid}$ with widths $w_1$ and $w_2$ designated as $w_{mid}$ and $w_{out}$, respectively. In the case of the auxiliary tapers, each comprises two sections labeled as $aux_1$ and $aux_2$ on the schematic. Each section possesses a length of $L_{aux_{1,2}}$ and $m_{aux}$. For $aux_1$, the widths $w_1$ and $w_2$ are $w_{aux_{tip}}$ and $w_{aux_{mid}}$, respectively, while for $aux_2$, these widths are swapped, resulting in a "Bowling Pin" shape for the auxiliary tapers.

One interesting result is that the wavelength at the middle of the range, 1.5 μm, which is typically the pumping signal wavelength, predominantly excited higher-order modes at the output waveguide. For an output waveguide with a width of 0.6 μm that supports only one mode at 1.5 μm, our coupler can facilitate the radiation of higher-order modes and effectively attenuate the coupling at the 1.5 μm wavelength. Due to optical reciprocity, the coupling from a 0.6-μm wide waveguide to a single-mode fiber would also be attenuated at 1.5 μm wavelength. This may be beneficial when coupling on-chip nonlinear broadband signals, *e.g.* octave-spanning frequency combs or supercontinuum to a fiber while simultaneously shaping its spectrum by reducing the coupling of the wavelengths around the pump where the intensity in the output spectrum peaks.

**Table 1. Parameters and dimensions of the design**

| Parameter | Description | Value |
|---|---|---|
| $w_{mid}$ | Tip width of the middle taper of the trident | 100 nm |
| $w_{auxtip}$ | Tip width of the auxiliary tapers of the trident | 150 nm |
| $w_{auxmid}$ | Middle width of the auxiliary tapers of the trident | 400 nm |
| $w_{out}$ | Width of the output waveguide | 0.6 μm |
| $SP_{mid}$ | The spacing between the midpoints of the auxiliary tapers | 2.4 μm |
| $\alpha$ | The angle of the auxiliary tapers with respect to the optical axis | 0.6° |
| $L_{mid}$ | The length of the middle taper | 30 μm |
| $L_{aux_{1,2}}$ | The length of section 1 or 2 of the auxiliary tapers | 18 μm |
| $m_{mid}$ | Taper profile factor of the middle taper | 0.5 |
| $m_{aux}$ | Taper profile factor of the auxiliary tapers | 1.9 |
| $L_{Design}$ | Total approximate length of the design | 37 μm |
| $W_{Design}$ | Total approximate width of the design | 3 μm |

OPTICS CONTINUUM

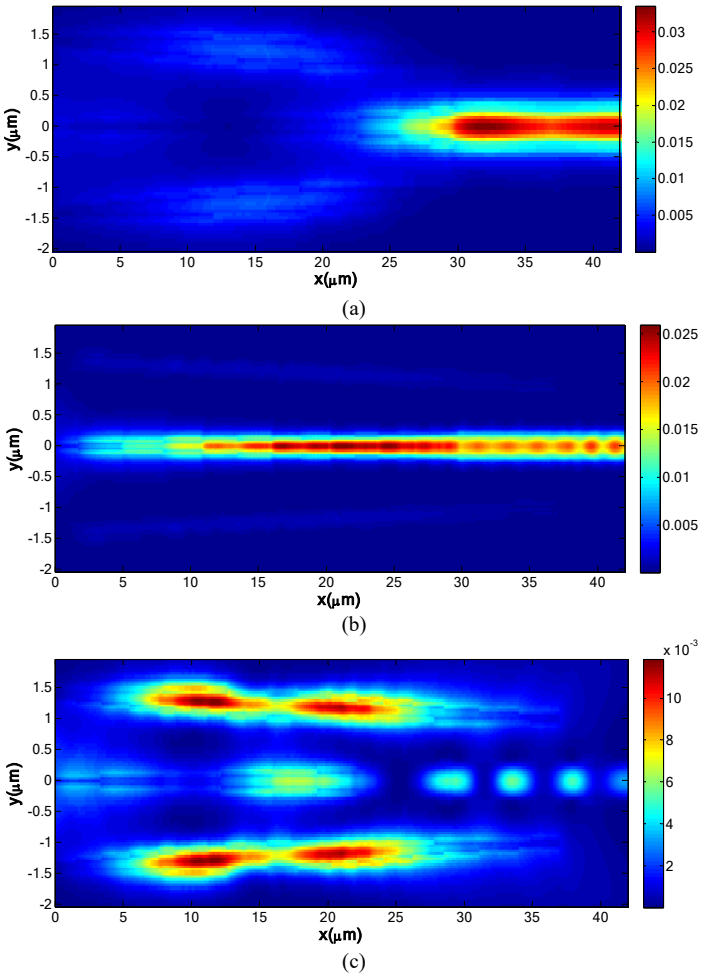


**Fig. 6.** Magnitude of the Poynting vector flowing through the structure from the edge of the trident towards the output waveguide. (a) For the spot at $\lambda = 2$ μm. (b) For the spot at $\lambda = 1$ μm. (c) For the spot at $\lambda = 1.5$ μm.

## 4. Results

In this section, the performance of the design and its tolerance are discussed. The design was simulated using commercial software Ansys Lumerical FDTD solution. The input spot from the lensed fiber was assumed to be Gaussian, with spot radii of 1 μm at $\lambda = 1$ μm, 1.5 μm at $\lambda = 1.5$ μm and 2 μm at $\lambda = 2$ μm. The waists of the Gaussians were assumed to be at the tip of the edge coupler.

### *4.1. Performance of the design*

In this section, we investigate the coupling efficiency between the input spot and the output waveguide, examining its wavelength-dependent variations around the central wavelengths. Our structure is designed to optimize coupling to the fundamental TE modes in the output waveguide. Figure 6 visually illustrates the magnitude of the Poynting vector, representing the power flow, from the trident's edge to the output waveguide. At $\lambda = 2$ μm (Fig. 6(a)), a substantial portion of the input spot is routed through auxiliary tapers via evanescent coupling. At $\lambda = 1$ μm (Fig. 6(b)),

OPTICS CONTINUUM

input power is mainly concentrated in the middle taper. Figure 6(c) shows that light at the intermediate wavelength of 1.5 μm radiates into higher-order modes, and results in significantly reduced transmission to the output waveguide which was intentionally engineered to exclusively support the fundamental mode.

Figure 7 presents the transmission spectra in the fundamental TE mode of the output waveguide for the three key spots: 1 μm (in dark red), 2 μm (in lime), and 1.5 μm (in purple). The spectra cover wavelength spans of ±10% around the center wavelengths. Comparing the proposed trident edge coupler design (solid lines) with the baseline using a single linear inverse taper (dashed lines) of 30-μm length and 130-nm tip width, it's clear that the trident coupler offers more optimized performance. Specifically, at the 1 μm and 2 μm wavelengths, the trident coupler achieves approximately 73% and 77% transmission, surpassing the linear taper's 70% and 67%, respectively. This signifies an average transmission improvement of about 10% for both spots when contrasted with the reference linear taper configuration. In addition, the trident coupler can attenuate the transmission at the 1.5 μm spot to about 6%, resulting in a remarkable reduction ratio of over 10 dB compared to the other two spots. In contrast, the linear taper allows the highest transmission at this wavelength, *i.e.,* the peak coupling is at 1.5 μm.

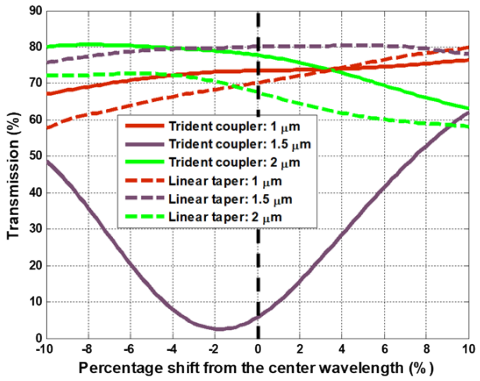


**Fig. 7.** Forward transmission to the fundamental TE mode of the output waveguide vs wavelength around the center wavelengths for the three key spots: 1 μm with a beam spot diameter of 2 μm (in dark red), 2 μm with a beam spot diameter of 4 μm (in lime), and 1.5 μm with a beam spot diameter of 3 μm (in purple). The solid lines are for the trident coupler and the dashed lines are for the single-tip linear inverse taper coupler.

Therefore, our trident coupler effectively splits the single taper's peak coupling at the intermediate wavelength (at 1.5 μm) into two distinct peaks, and one can engineer the wavelengths of these two peak couplings and align them precisely to the desired wavelengths of 1 μm and 2 μm. Figure 8 illustrates the forward transmission versus wavelength for both couplers, assuming a linear relationship between the spot radius and the wavelength for an extended range of 0.75-2.25 μm, which is beyond the range of interest in this manuscript but could be useful for other applications. This graph showcases a band-stop-like response for the trident coupler, which can aid in partially equalizing any bell-shaped spectrum. It also demonstrates that the trident coupler exhibits better coupling compared to the linear taper for spots outside the range of 1-2 μm, rendering it suitable for coupling a broader range than the single taper. We believe that in applications where the output spectrum peaks around the middle wavelength, typically associated with the pump, our trident coupler offers distinctive advantages over conventional single-tip tapers in shaping the spectrum during the coupling of light. Meanwhile, if all wavelengths are to be coupled in/out without spectral shaping, a single-tip coupler may still be preferred.

OPTICS CONTINUUM

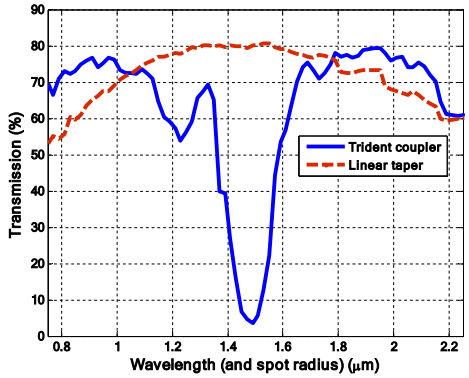


**Fig. 8.** Forward transmission to the fundamental TE mode of the output waveguide vs wavelength (and spot radius) for both couplers. Linear variation is assumed between the spot radius and the wavelength. For example, light at a wavelength of 0.75μm has a spot radius of 0.75 μm while light at a wavelength of 2.25 μm has a spot radius of 2.25 μm.

### *4.2. Tolerance to focal distance, spot size variations and fiber misalignment*

The alignment of a lensed fiber to the chip is a challenging task due to the small size of the input spot and the chip's dimensions. Moreover, the output spot size from the lensed fiber may exhibit variations. Therefore, there is a need for an edge coupler that can withstand these variations in the output spot size and remain tolerant to misalignments of the fiber. This section focuses on examining the design's resilience to such misalignments and variations, addressing the critical issue of robustness in optical coupling.

As discussed in the previous section, we assumed that the focal distances of both 1 μm and 2 μm wavelengths are identical, and here we look into the cases where they are at different distances which results from many factors including the different MFDs and the chromatic dispersion at the two wavelengths.

Figure 9 illustrates the tolerance of the design to variations in the position of the waist of the input Gaussian beam, which corresponds to shifts of the fiber along its axis. The forward transmission is plotted against the position of the waist concerning the edge of the trident, with shifts spanning ±1 μm. The analysis reveals the design's remarkable insensitivity, as it consistently maintains forward transmissions exceeding 75% and 66% at $\lambda = 2$ μm and $\lambda = 1$ μm, respectively, as shown in Fig. 9(a), and a reduced forward transmission less than 10% at $\lambda = 1.5$ μm, as shown in Fig. 9(b).

Figure 10 further demonstrates the design's resilience, showcasing the forward transmission versus the percentage change in the input spot size. Here, the design exhibits a high tolerance for both spots of interest, with forward transmissions consistently surpassing 75% and 69% at $\lambda = 2$ μm and $\lambda = 1$ μm, respectively, even when subjected to changes of up to 10% in the spot sizes, as depicted by Fig. 10(a). Figure 10(b) demonstrates that the spot at $\lambda = 1.5$ μm will consistently exhibit reduced coupling, remaining below 7%, even with variations of up to 10% in its spot size. These results highlight the design's robustness in accommodating variations in the input Gaussian beam's position and size for all the considered spots.

Figures 11 and 12 explore the design's tolerance to misalignments of the input fiber at the different wavelengths, considering shifts of up to ±1 μm. Figure 11 illustrates the forward transmission to the fundamental TE mode concerning in-plane shifts (parallel to the chip) of the fiber, while Fig. 12 focuses on the forward transmission with respect to out-of-plane shifts (perpendicular to the chip). It's worth noting from Fig. 11(a) and Fig. 12(a) that the spot at $\lambda = 2$ μm, due to its larger size, exhibits a higher tolerance to misalignments. Both spots, however,

OPTICS CONTINUUM

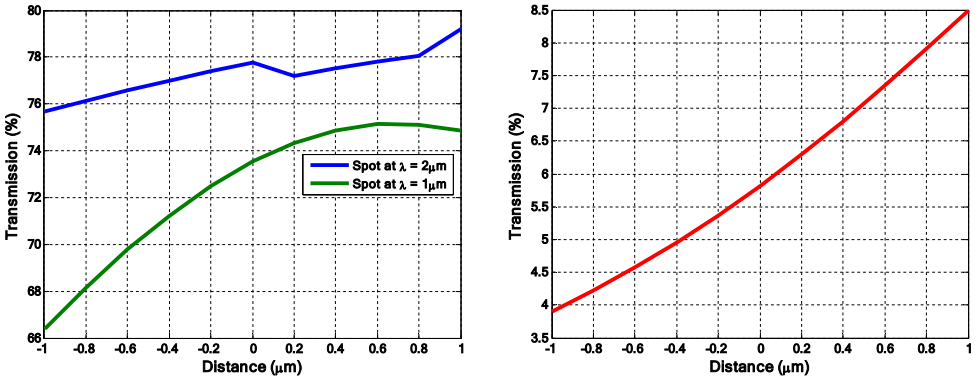


**Fig. 9.** Forward transmission to the fundamental TE mode vs the position of the waist of the Gaussian beam with respect to the edge of the trident. (a) For the spots at $\lambda = 2$ μm and $\lambda = 1$ μm. (b) For the spot at $\lambda = 1.5$ μm.

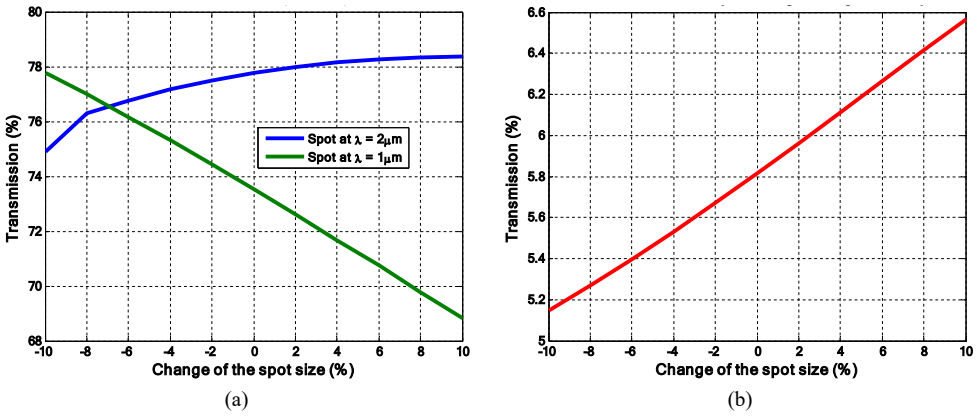


**Fig. 10.** Forward transmission to the fundamental TE mode vs the percentage change of the input spot size. (a) For the spots at $\lambda = 2$ μm and $\lambda = 1$ μm. (b) For the spot at $\lambda = 1.5$ μm.

maintain reasonable forward transmissions (>50%) even with shifts of up to ±0.5 μm. Moreover, they maintain forward transmissions of >15% even when subjected to shifts as significant as ±1 μm. Figure 11(b) and Fig. 12(b) demonstrate that the spot at $\lambda = 1.5$ μm will consistently exhibit reduced coupling, remaining below 8%. These findings highlight the robustness of the design in accommodating misalignments of the input fiber for the larger spot, which is a critical feature in practical applications where precise alignment can be challenging. However, further improvements might be required to enhance the misalignment sensitivity for the smaller spot. Our design maintains a comparable tolerance to variations in focal distance, spot size, and fiber misalignments when compared to the inverse single taper.

### *4.3. Tolerance to the fabrication variations*

In addition to the necessity for the design to tolerate misalignments and variations in the input fiber, it must also exhibit tolerance to fabrication variations. The fabrication process is inherently subject to various sources of nonuniformity, resulting in structures that are thinner or wider than initially designed. The areas that are most susceptible to these variations are typically those with the smallest dimensions, which, in this design, are the tips of the trident tapers.

OPTICS CONTINUUM

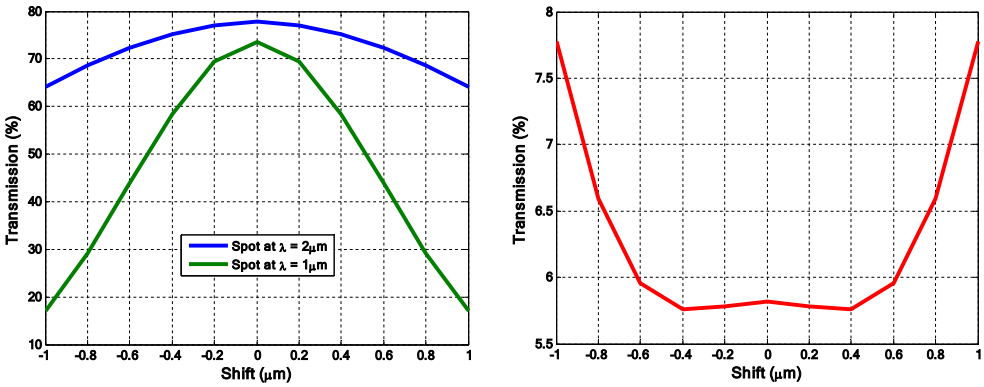


**Fig. 11.** Forward transmission to the fundamental TE mode vs the in-plane shift (parallel to the chip) of the input spot. (a) For the spots at $\lambda = 2$ μm and $\lambda = 1$ μm. (b) For the spot at $\lambda = 1.5$ μm.

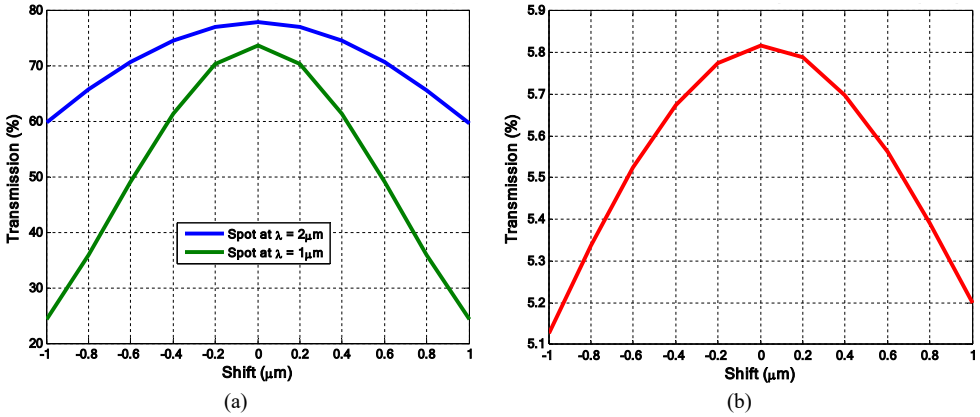


**Fig. 12.** Forward transmission to the fundamental TE mode vs the out-of-plane shift (perpendicular to the chip) of the input spot. (a) For the spots at $\lambda = 2$ μm and $\lambda = 1$ μm. (b) For the spot at $\lambda = 1.5$ μm.

OPTICS CONTINUUM

Figure 13 illustrates the forward transmission to the fundamental TE mode as a function of changes in the tip widths of the trident tapers (solid lines) and compares them with the single linear taper (dashed lines) for the different wavelengths. Specifically, the tip widths of three tapers (the middle taper and the auxiliary ones) of the trident coupler, as well as the tip width of the reference single taper, are assumed to vary by ±50 nm around their nominal values. Notably, as depicted by Fig. 13(a), the trident coupler exhibits a robust tolerance to such fabrication variation for the two spots at $\lambda = 2$ μm and $\lambda = 1$ μm, maintaining forward transmissions exceeding 70% and 65% at $\lambda = 2$ μm and $\lambda = 1$ μm, respectively. In contrast, the linear taper's coupling can deteriorate to below 55% for the smaller spot and below 60% for the larger spot. In the case of the spot at $\lambda = 1.5$ μm, illustrated in Fig. 13(b), the coupling in the trident configuration reduces as the tip widths decrease. However, the coupling starts to increase as the tip widths increase, albeit still maintaining reduced coupling compared to the corresponding single taper case by >21 dB and >3 dB in the best and worst cases, respectively. If a high fabrication tolerance is anticipated, it might be feasible to adjust the tip widths to values slightly lower than the nominal points to ensure reduced coupling at the spot at $\lambda = 1.5$ μm. This robust performance underscores the design's fabrication-friendliness and highlights its suitability for practical applications where manufacturing variations are unavoidable.

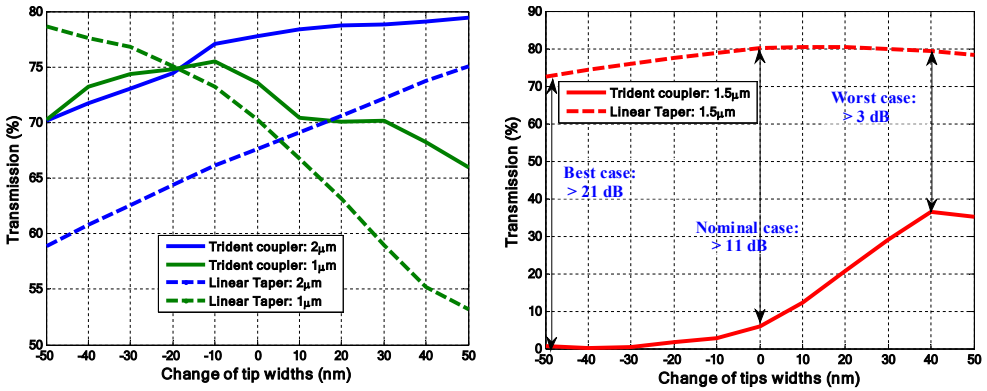


**Fig. 13.** Forward transmission to the fundamental TE mode vs the change in the tip widths. (a) For the spots at $\lambda = 2$ μm and $\lambda = 1$ μm. (b) For the spot at $\lambda = 1.5$ μm. The solid lines are for the trident coupler and the dashed lines are for the single-tip linear inverse taper coupler.

Finally, we discuss the feasibility of fabrication for our design. The current main challenge is the extremely high aspect ratio of 1:6 at the tip of the taper, *i.e.* 100 nm width and 600 nm height. While such aspect ratios can be achieved in other materials such as silicon and silicon nitride, the current etching technology of LN does not appear to accommodate such a configuration. One way to reduce the aspect ratio is to introduce metamaterial structures [20] to maintain the low effective index at the tip of the inverse taper while employing larger widths.

To demonstrate the adaptability of the proposed design to different dimensions dictated by fabrication constraints and side wall angles, the thickness of the LN film was adjusted to 400 nm, and the minimum width in the design was set to 150 nm (which represents the width at the intermediate height of the structure when considering the sidewall angles), thus reducing the maximum aspect ratio from 1:6 to 1:2.7. By making a few modifications to the original design, *i.e.*, setting $w_{mid} = 150$ nm, $w_{aux_{tip}} = 250$ nm, $w_{aux\,mid} = 450$ nm, $SP_{mid} = 2.2$ m m and $m_{aux} = 3$ while keeping all other parameters, the trident coupler would achieve approximately 71% and 73% transmission at wavelengths of 1 μm and 2 μm, respectively. This performance compares favorably to 65% and 63% transmission, respectively, for the baseline, *i.e.*, an optimized single

OPTICS CONTINUUM

inverse taper with a tip width of 150 nm and taper length of 20 µm. Furthermore, the trident coupler would exhibit a reduced transmission of approximately 10% at 1.5 µm as compared to 77% for the corresponding baseline, demonstrating a similar level of functionality versus the design for 600 nm thickness. In practical scenarios where the fabrication process and its associated constraints, such as maximum film thickness, sidewall angles and minimum features are known, the coupler design can be optimized following the same procedure in this paper to achieve peak performance based on these constraints.

## 5. Conclusion

In conclusion, we have presented the design and performance evaluation of a trident edge coupler configured on a 600-nm-thick X-cut LNOI with a footprint of approximately 37 µm by 3 µm for octave-spanning broadband coupling. This carefully designed coupler can efficiently couple light from a nonlinear waveguide to a lensed fiber at specific wavelengths, $\lambda = 2$ µm and $\lambda = 1$ µm, while simultaneously attenuating the coupling of the wavelength at the middle, *i.e.* 1.5 µm.

A theoretical estimation of the lensed fiber focal spot sizes at the two wavelengths was presented, and the spot diameters of 4 µm and 2 µm were used at $\lambda = 2$ µm and $\lambda = 1$ µm, respectively. Through simulation, we showed that the coupling losses are less than 1.4 dB for both spots. Notably, peak forward transmissions of approximately 73% and 77% were achieved at the 1 µm and 2 µm wavelength spots, respectively. This resulted in an average transmission enhancement of nearly 10% compared to the average performance of a single linear taper at the two spots. Interestingly, we achieved significant attenuation of a 1.5 µm pump, with a reduction ratio exceeding 10 dB when compared to the 1 µm and 2 µm spots.

Moreover, the design demonstrates significant robustness by showcasing tolerance to variations in the input spot's focal position along the axis and to the changes in its size. Additionally, it exhibits enhanced tolerance to variations in the tip widths of the trident tapers, stemming from fabrication-related variations, when compared to that of the single taper. Moreover, the design can be tailored to suit different configurations and film thicknesses, accounting for variations in sidewall angles and minimum feature sizes. Furthermore, the design sustains a reasonable tolerance to both in-plane and out-of-plane shifts of the input spot, further reinforcing its reliability in practical applications.

In applications related to broadband fiber-to-chip coupling, where the intensity of the output spectrum peaks around the middle wavelength, our trident coupler presents distinctive advantages over conventional single-tip tapers in shaping the spectrum during the coupling of light for subsequent optical signal manipulation devices on a heterogeneous material integrated platform. Such a platform may entail the generation of broadband light on one chip and the subsequent manipulation of signals on another chip. Thus, efficient coupling between them becomes necessary.

**Funding.** National Science Foundation (DMR-2323752); Defense Advanced Research Projects Agency (APhI program).

**Acknowledgments.** The effort at Purdue under the DARPA APhI program was part of a project team led by Sandia National Laboratories.

**Disclosures.** The authors declare no conflicts of interest.

**Data availability.** Data underlying the results presented in this paper are not publicly available at this time but may be obtained from the authors upon reasonable request.

## References

1. P. Del'Haye, A. Schliesser, O. Arcizet, *et al.*, "Optical frequency comb generation from a monolithic microresonator," Nature **450**(7173), 1214–1217 (2007).
2. C. V. Poulton, M. J. Byrd, M. Raval, *et al.*, "Large-scale silicon nitride nanophotonic phased arrays at infrared and visible wavelengths," Opt. Lett. **42**(1), 21–24 (2017).

OPTICS CONTINUUM


3. S.-M. Kim, E.-S. Lee, K.-W. Chun, *et al.*, "Compact solid-state optical phased array beam scanners based on polymeric photonic integrated circuits," Sci. Rep. **11**(1), 10576 (2021).
4. H. Hashemi, "A review of silicon photonics LiDAR," in *2022 IEEE Custom Integrated Circuits Conference (CICC)* (2022), pp. 1–8.
5. R. S. El Shamy, D. Khalil, and M. A. Swillam, "Mid infrared optical gas sensor using plasmonic Mach-Zehnder interferometer," Sci. Rep. **10**(1), 1293 (2020).
6. R. S. El Shamy, M. A. Swillam, and X. Li, "On-chip complex refractive index detection at multiple wavelengths for selective sensing," Sci. Rep. **12**(1), 9343 (2022).
7. J. Feldmann, N. Youngblood, M. Karpov, *et al.*, "Parallel convolutional processing using an integrated photonic tensor core," Nature **589**(7840), 52–58 (2021).
8. Y. Tang, P. T. Zamani, R. Chen, *et al.*, "Device-system end-to-end design of photonic neuromorphic processor using reinforcement learning," Laser Photonics Rev. **17**(2), 2200381 (2023).
9. D. Marpaung, J. Yao, and J. Capmany, "Integrated microwave photonics," Nat. Photonics **13**(2), 80–90 (2019).
10. N. P. O'Malley, K. A. McKinzie, M. S. Alshaykh, *et al.*, "Architecture for integrated RF photonic downconversion of electronic signals," Opt. Lett. **48**(1), 159–162 (2023).
11. R. Rady, C. Madsen, S. Palermo, *et al.*, "A 20–43.5-GHz wideband tunable silicon photonic receiver front-end for mm-wave channel selection/jammer rejection," J. Lightwave Technol. **41**(5), 1309–1324 (2023).
12. D. Zhu, L. Shao, M. Yu, *et al.*, "Integrated photonics on thin-film lithium niobate," Adv. Opt. Photonics **13**(2), 242–352 (2021).
13. M. Levy, R. M. Osgood Jr, R. Liu, *et al.*, "Fabrication of single-crystal lithium niobate films by crystal ion slicing," Appl. Phys. Lett. **73**(16), 2293–2295 (1998).
14. P. Rabiei and P. Gunter, "Optical and electro-optical properties of submicrometer lithium niobate slab waveguides prepared by crystal ion slicing and wafer bonding," Appl. Phys. Lett. **85**(20), 4603–4605 (2004).
15. M. Yu, B. Desiatov, Y. Okawachi, *et al.*, "Coherent two-octave-spanning supercontinuum generation in lithium-niobate waveguides," Opt. Lett. **44**(5), 1222–1225 (2019).
16. L. Cheng, S. Mao, Z. Li, *et al.*, "Grating couplers on silicon photonics: design principles, emerging trends and practical issues," Micromachines **11**(7, 666 (2020).
17. X. Mu, S. Wu, L. Cheng, *et al.*, "Edge couplers in silicon photonic integrated circuits: a review," Appl. Sci. **10**(4), 1538 (2020).
18. J. Wang, Y. Xuan, C. Lee, *et al.*, "Low-loss and misalignment-tolerant fiber-to-chip edge coupler based on double-tip inverse tapers," *2016 Optical Fiber Communications Conference and Exhibition, OFC 2016 7*, 6–8 (2016).
19. M. Teng, B. Niu, K. Han, *et al.*, "Trident shape SOI metamaterial fiber-to-chip edge coupler," in *Optical Fiber Communication Conference (OFC) 2019*, OSA Technical Digest (Optica Publishing Group, 2019), p. Tu2J.6.
20. A. He, X. Guo, T. Wang, *et al.*, "Ultracompact fiber-to-chip metamaterial edge coupler," ACS Photonics **8**(11), 3226–3233 (2021).
21. X. Liang, L. Fu, Q. Yu, *et al.*, "Efficient and broadband trident spot-size convertor for thin-film lithium niobate integrated device," IEEE Photonics Technol. Lett. **35**(1), 35–38 (2023).
22. S. H. Tao, J. Song, Q. Fang, *et al.*, "Improving coupling efficiency of fiber-waveguide coupling with a double-tip coupler," Opt. Express **16**(25), 20803–20808 (2008).
23. Y. Zhang, S. Yang, A. E.-J. Lim, *et al.*, "A compact and low loss Y-junction for submicron silicon waveguide," Opt. Express **21**(1), 1310–1316 (2013).
24. J. R. Ong, T. Y. L. Ang, G. Alagappan, *et al.*, "Silicon nitride double-tip fiber-to-waveguide edge couplers at visible wavelengths," *Optics InfoBase Conference Papers Part F122-*, 4–6 (2017).
25. J. O. Gerguis, G. Chang, M. I. Abdelrahman, *et al.*, "MMI-based power combiner for trident edge couplers on thin film lithium niobate for nonlinear applications," in *CLEO 2023*, Technical Digest Series (Optica Publishing Group, 2023), p. JW2A.32.
26. OzOptics, "Tapered and Lensed Fibers," https://www.ozoptics.com/ALLNEW_PDF/DTS0080.pdf.
27. C. Wang, M. Zhang, M. Yu, *et al.*, "Monolithic lithium niobate photonic circuits for Kerr frequency comb generation and modulation," Nat. Commun. **10**(1), 978 (2019).
28. D. Marcuse, "Loss analysis of single-mode fiber splices," The Bell Syst. Tech. J. **56**(5), 703–718 (1977).
29. B. E. A. Saleh and M. C. Teich, "Beam optics," in Fundamentals of Photonics (1991), pp. 80–107.